Results in Optics 14 (2024) 100611

Contents lists available at ScienceDirect

Results in Optics

journal homepage: www.sciencedirect.com/journal/results-in-optics

Optimization of formamidinium-based perovskite solar cell using SCAPS-1D

David Ompong [a,b,*], Michelle Clements [a]

[a] Faculty of Science & Technology, Charles Darwin University, 0909 Darwin, NT, Australia
[b] Energy and Resources Institute, Charles Darwin University, 0909 Darwin, NT, Australia

ARTICLE INFO

Keywords:
Active layer optimization
Formamidinium lead iodide perovskite
Perovskite solar cells
SCAPS-1D simulation

ABSTRACT

Perovskite materials have recently emerged as promising candidates as an absorber layer in solar cells. In this study, the photovoltaic performance of a formamidinium lead iodide perovskite ($FAPbI_3$) based solar cell is assessed and improved by optimizing the thickness of the active layer using the Solar Cell Capacitance Simulator (SCAPS-1D) software. The architecture of the solar cell analyzed is a conventional planar n-i-p type composed of fluorine-doped tin oxide (FTO) as the front contact, tin oxide (SnO2) as the electron transport layer (ETL), $FAPbI_3$ as the absorber layer, lithium bis(trifluoromethylsul-phonyl)imide (LiTFSI) doped spiro-OMeTAD as the hole transport layer (HTL), and silver (Ag) as the back contact. The simulation was carried out with and without parasitic resistances. The efficiency of the ideal device was 20.95 % when absorber thickness was between 0.68 μm and 0.78 μm and 14.45 % for the non-ideal device when the series resistance $\boldsymbol{R_{series}} = 10\ \Omega{\cdot}cm^2$ and shunt resistance $\boldsymbol{R_{shunt}} = 5000\ \Omega{\cdot}cm^2$. We have found that the PCE of the original non-ideal device can be increased by 26 % through optimization of layer thickness and carrier transport.

1. Introduction

The current solar cell industry is dominated by silicon-based devices. However, perovskite solar cells (PSCs) have gained much research interest in recent years because their excellent photophysical and electrical properties and relatively easy fabrication (Manser et al., 2016); (Shao and Loi, 2020), and (Djurisic, 2017). The rapid improvement in the power conversion efficiency (PCE) of PSCs make them potential candidates for an emerging third-generation photovoltaic industry. High PCE makes commercializing PSCs very appealing. However, a desirable combination of high PCE, low fabrication cost, large-scale fabrication method and long-term stability are required for the PSCs commercialization to begin (Ono, 2017; Song, 2016; Whalley, 2017).

The presence of lead, which is toxic, in the hybrid organic–inorganic metal lead perovskites and the lack of long-term structural stability of PSCs to light and heat are some of the pressing challenges hindering PSCs commercialization (Ono, 2017; Ding, 2022), because long-term stability is a requirement for practical application of PSCs. Tin-based PSCs can address the former challenge, albeit with a lower PCE, and various stabilization strategies such as cation or halide engineering and substituting elements such as Sn, Bi, and Cu, etc. can improve the later (Karthick et al., 2021). Despite the high PCE, PSCs have not reached the ideal Shockley–Queisser limit of single-junction solar cells at standard test conditions (Mercaldo, 2022).

Thus, the device performance can improve further by optimizing the PSCs parameters. Several theoretical and experimental studies have been carried out to investigate new pathways to improve the performance and stability of PSCs such as using $FAPbI_3$ instead of $MAPbI_3$ as the absorber layer to reduce the rotational degree of freedom of FA and prolong its lifetime (Gelvez-Rueda et al., 2017). A comparative study on the photovoltaic performance of CH3NH3PbI3- and CH3NH3SnI3-based PSCs by optimizing the different layer thicknesses using SILVACO ATLAS simulation software and found PCE of 18.16 % and 9.56 %, respectively (Hima, 2019). Experimentally, PSCs of different nano-textured front surfaces were studied to find the devices with optimum efficiency compared with the planar device. Using a combination of Cos − nanotextures and a sodium fluoride antireflective coating, PCE of 19.7 % was achieved when compared to the planar device (Tockhorn, 2020). The addition of cesium ($Cs+$) and bromine ($Br-$) to $FAPbI_3$ based device increased the PCE from 4 to 15 % under standard illumination condition (Karthick et al., 2020).

The emergence of perovskite absorber materials and hole transport layers (HTLs) are revolutionizing the emerging perovskite photovoltaic technologies (Hao, 2014). Hole transport layers are important for

* Corresponding author.

https://doi.org/10.1016/j.rio.2024.100611
Received 15 November 2023; Accepted 21 January 2024
Available online 24 January 2024

efficient charge carrier extraction (Li, 2020) and achieving high PCE and stability in PSCs (Głowienka, 2020; Ompong and Singh, 2018). Factors such as absorption profile, HOMO energy level, electrical conductivity, and hole mobility are important parameters to evaluate the potential of a HTL in a PSC. The HTL facilitates interfacial hole transport and suppression of the interfacial charge recombination. The hole mobility in HTL was increased by doping spiro-OMeTAD with Lithium bis(trifluoromethylsulphonyl)imide (LiTFSI) and 2,6-lutidine dopant during the fabrication process (Hao, 2014). About a 100-fold increase in hole mobility compared with the pristine of LiTFSI-doped spiro-OMeTAD is confirmed experimentally through impedance spectroscopy (Li, 2020). The bandgap of the LiTFSI-doped spiro-OMeTAD is also slightly larger $E_g = 3.17$ eV (Hao, 2014), compared with the pristine spiro-OMeTAD $E_g = 2.9$ eV (Karthick et al., 2020).

In this study, the optimized thickness required for a formamidinium lead iodide perovskite ($FAPbI_3$) absorber sandwiched between hole transport layer (HTL) and electron transport layer ETL, with FTO and Ag as front and back contacts, respectively, has been analyzed. The contextual understanding of PSC characteristics such as parasitic resistances, diffusion length, charge generation, charge mobility, charge carrier lifetime, and defect concentration has been studied. The absorber layer thickness was first optimized and further analysis was carried out to help fully understand the device parameters. By considering the device as ideal, we were first able to evaluate the optimal operational limits of the device. Then, characteristics of the non-ideal device such as parasitic resistances were introduced to simulate a more realistic solar cell and a comparison between the theoretical and experimental results have been made. The PSC structure studied here differs from the one (D-A) in Karthick et al., (Karthick et al., 2020) by the LiTFSI-doped spiro-OMeTAD with higher hole mobility and bandgap and the Ag metal contact instead of Au.

2. Devicestructure and simulation methodology

The Solar Cell Capacitance Simulator One Dimensional (SCAPS-1D) software (Burgelman et al., 2000) is used in this study. SCAPS-1D was chosen for its availability and usability on a window application. SCAPS simulation is mainly derived from three fundamental equations: Poisson equation, hole cotinuity equation, and electron continuity equation.

2.1. Dvice architecture

A planar n-i-p PSC structure consisting of: fluorine-doped tin oxide (FTO) (as front contact)/SnO_2 (ETL)/$FAPbI_3$ (light absorber)/spiro-OMeTAD:LiTFSI (HTL)/Silver (Ag) (back contact) as shown in Fig. 1 was studies. The flat band energy diagram of the device architecture is shown in Fig. 2. The input parameters of ETL, active layer, and HTL were selected from experimental and theoretical results from published literature and are shown in Table 1.

Tin oxide (SnO_2) was selected as the ETL due to the high electron mobility and conductivity, broad optical bandgap, which means most photons will pass through the ETL and be absorbed in the active layer, low temperatures deposition process, appropriate energy alignment at the ETL/perovskite interface, and excellent stability under UV illumination. This configuration causes different ETL layer thicknesses to change the fraction of light transmitted to the absorber and in general the deposited SnO_2 is thicker than TiO_2 as discussed by Karthick *et. al.* (Karthick et al., 2020).

Parameters such as the thermal velocity of electrons and holes was set to 1.0 x 10^7cm·s^{-1} (Karthick et al., 2020); (Du et al., 2016); (Abdelaziz, 2020). The radiative recombination rate in the absorber layer was extracted from (Gelvez-Rueda et al., 2017) as 3.50 × $10^{-9}$$cm^{-3}$. The radiative recombination rate is reported at 20 °C and while our simulation operates at a slightly higher temperature, the difference is not expected to have a high impact on the results.

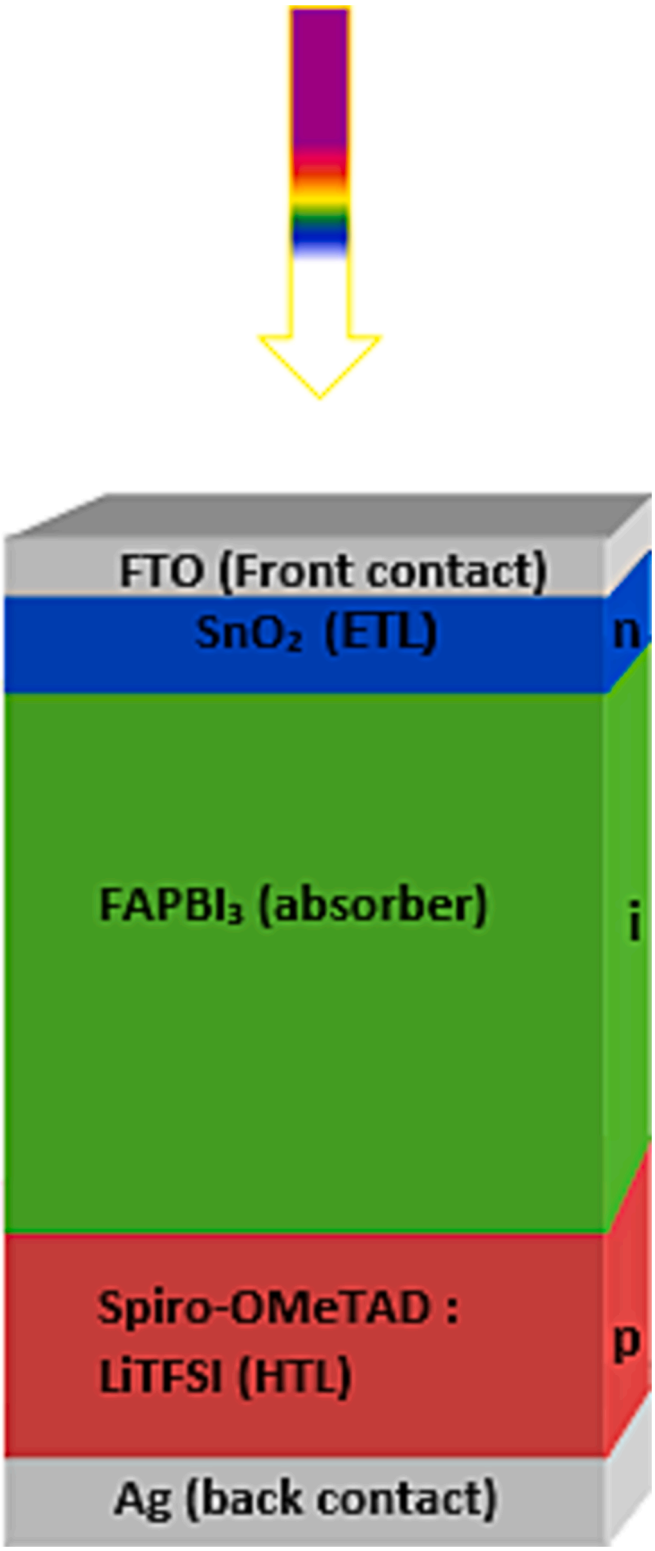

Fig. 1. Schematic diagram of the planar n-i-p perovskite solar cell device architecture.

The interface defect densities influencing the charge carrier recombination at the ETL/perovskite and perovskite/HTL interfaces used in this study are listed in Table 2.

The metal work function of the front and back contacts was set to be 0.12 eV above the E_V and 0.4 eV below the E_C, respectively.

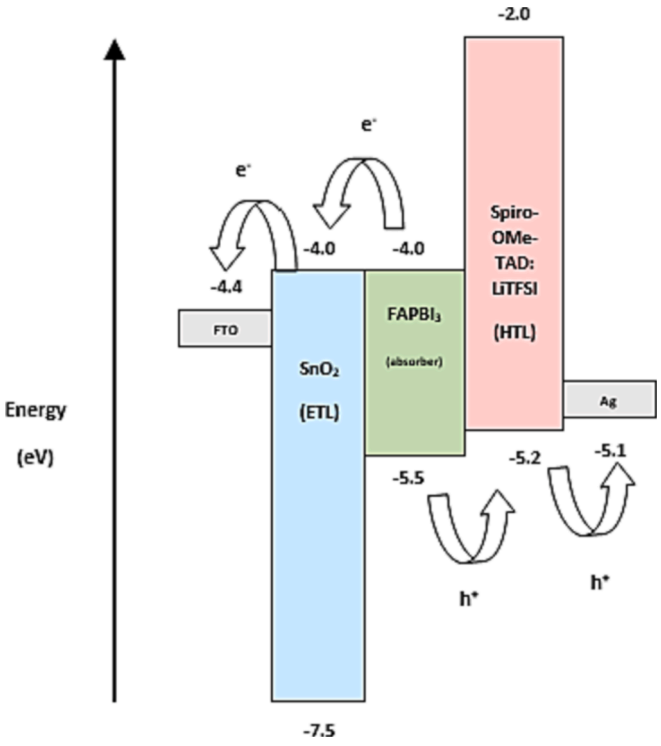

Fig. 2. Simplified flat band energy diagram of FTO, ETL, HTL, $FAPbI_3$ absorber, and Ag is shown along with the expected charge transfer processes of electrons and holes (figure (); ().).
adapted from Hao, 2014Karthick et al., 2020

2.2. Ideal and non-ideal devices

In this simulation study, the device without considering any series or shunt resistances (ideal) is first optimized. Although a non-realistic model, this step helps to ascertain the highest possible limit of the device performance. The series resistance was varied from 10 to 100 $\Omega{\cdot}cm^2$, while the shunt resistance was varied from 500 to 5000 $\Omega{\cdot}cm^2$ to understand the effects of series and shunt resistances on device performance. This range of values was selected based on experimental results shown in (Karthick et al., 2020) for several planar formamidinium perovskite solar cells; where the series resistance was generally less than 100 $\Omega{\cdot}cm^2$ and the shunt resistance was always greater than 500 $\Omega{\cdot}cm^2$.

2.3. Simulation

The device structure using the layer parameters listed in Tables 1 and 2 was built in SCAPS-1D. Considering the p-type and n-type regions of a diode as infinite sheets, it can be considered as a 1D object which greatly simplifies the equations used for the modelling. The single diode model of an n-i-p diode structure illuminated from the right is shown in Fig. 3. The simulation was carried out at a temperature of 300 K under AM1.5G solar illumination spectrum with an incident light power of 1000 W/m^2 (Karthick et al., 2021; Rahman, et al., 2019); (De Los Santos, 2020). The J–V curves for the device were simulated over the voltage range of 0–2 V.

In SCAPS-1D, using the batch parameter settings, the thickness of each layer in the PSC can be varied. The absorber thickness was varied from 0.2 μm to 2.0 μm in the batch mode. Once the optimal absorber thickness was found, the recorder mode was again enabled varying the series resistance from 10 to 100 $\Omega{\cdot}cm^2$ and the shunt resistance from 500 to 5000 $\Omega{\cdot}cm^2$.

Table 1
Details of input parameters used for the simulation.

Parameter	SnO_2	$FAPbI_3$	Spiro-OMeTAD: LiTFSI
Thickness (ηm)	70 (Karthick et al., 2020)	200-2000[a]	200 (Du et al., 2016)
Band gap (eV)	3.5 (Karthick et al., 2020)	1.47 (Ma, 2017)	3.17 (Hao, 2014)
electron affinity (eV)	4 (Karthick et al., 2020)	4 (Karthick et al., 2020)	2.05 (Hao, 2014)
Dielectric permittivity (relative)	9 (Karthick et al., 2020)	6.6 (Karthick et al., 2020); (Chen et al., 2016)	3 (Du et al., 2016); (Abdelaziz, 2020)
CB effective density of states (cm^{-3})	2.2 x 10^{17} (Karthick et al., 2020)	1.2 x 10^{19} (Karthick et al., 2020)	2.2 x 10^{18} (Du et al., 2016); (Abdelaziz, 2020)
VB effective density of states (cm^{-3})	2.2 x 10^{17} (Karthick et al., 2020)	2.9 x 10^{18} (Karthick et al., 2020)	1.8 x 10^{19} (Du et al., 2016); (Abdelaziz, 2020)
e^- thermal velocity, ($cm{\cdot}s^{-1}$)	1.0 x 10^7 (Karthick et al., 2020)	1.0 x 10^7 (Karthick et al., 2020)	1.0 x 10^7 (Du et al., 2016); (Abdelaziz, 2020)
h^+ thermal velocity ($cm{\cdot}s^{-1}$)	1.0 x 10^7 (Karthick et al., 2020)	1.0 x 10^7 (Karthick et al., 2020)	1.0 x 10^7 (Du et al., 2016); (Abdelaziz, 2020)
Mobility of e^-, μ_n ($cm^2{\cdot}v^{-1}{\cdot}s^{-1}$)	20 (Karthick et al., 2020)	2.7 (Karthick et al., 2020); (Gelvez-Rueda et al., 2017)	2.0 x 10^{-4} (Du et al., 2016); (Abdelaziz, 2020)
Mobility of h^+, μ_p ($cm^2{\cdot}v^{-1}{\cdot}s^{-1}$)	10 (Karthick et al., 2020)	1.8 (Karthick et al., 2020); (Gelvez-Rueda et al., 2017)	1.0 x10^{-4} (Li, 2020)
Density of n-type doping, N_D (cm^{-3})	1.0 x 10^{15} (Karthick et al., 2020)	1.3 x 10^{16} (Karthick et al., 2020)	0 (Du et al., 2016); (Abdelaziz, 2020)
Density of p-type doping, N_A (cm^{-3})	0 (Karthick et al., 2020)	1.3 x 10^{16} (Karthick et al., 2020)	2.8 x 10^{19} (Li, 2020)
Density of defects, N_t (cm^{-3})	1.0 x 10^{18} (Karthick et al., 2020)	9 x 10^{14} (Gelvez-Rueda et al., 2017)	1.0 x 10^{15} (Du et al., 2016); (Abdelaziz, 2020)

[a] Indicates this work.

Table 2
Interface defect densities.

Parameter	ETL/absorber	Absorber/HTL
Defect type	neutral	neutral
Capture cross section for e^- and h^+ (cm^2)	1 x 10^{-15} (Abdelaziz, 2020)	1 x 10^{-15} (Abdelaziz, 2020)
Energetic distribution	Single (Abdelaziz, 2020)	Single (Abdelaziz, 2020)
Energy level with respect to Ev	0.6	0.6
Total density (cm^{-2})	2 x 10^{11} (Chouhan et al., 2018)	5 x 10^8 (Chouhan et al., 2018)

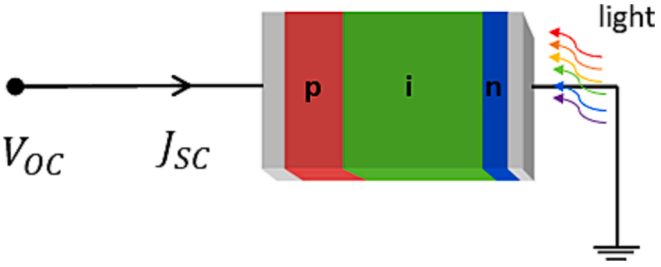

Fig. 3. PSC simulation setup: illumination from the right and J_{sc} considered positive when entering left contact.

3. Results and discussion

3.1. Simulation of ideal device

We have taken all the basic parameters as per Tables 1 and 2. The effect of varying the absorber layer thickness on the open-circuit voltage V_{OC}, fill factor FF, , short-circuit current density J_{SC}, and PCE η, of an ideal device is shown in Fig. 4, Fig. 5, Fig. 6, and Fig. 7, respectively. As mentioned earlier, the device was first considered without any series or shunt resistances. Hence the overall device performance was first found independent from the electrical losses occurring in non-ideal devices.

Fig. 4 highlights that the ideal device can reach an open-circuit voltage of 0.929 V when the absorber thickness is between 0.76 μm and 0.86 μm. The fill factor steadily decreases from 86 % to 61 % as the absorber thickness increases as shown in Fig. 5. Fig. 6 show that the short-circuit current density increases from 19 mA/cm^2 at a thickness of 0.2 μm until it plateaus at a value of 29 mA/cm^2 once an absorber thickness of 1.32 μm is reached.

The maximum efficiency of the ideal device is 20.95 % to an absorber thickness between 0.68 μm and 0.78 μm as shown in Fig. 7. Increasing the layer thickness means more material of the active layer is exposed to light and therefore more electron-hole pairs are created. The decreasing FF can be understood as the result of short life-time of mobile charge carriers and the associated internal recombination inside perovskite material with increasing active layer thickness.

3.2. Simulation of the non-ideal device

After optimizing the thickness of the absorber layer of the ideal device, parasitic resistances were introduced. Parasitic resistances have a huge impact on the photovoltaic performance of a device because they govern the shape and slopes of the J-V characteristics. The series resistance R_{series}, comes from the electrical resistance associated with the materials and contacts of the device and it mainly affects the FF and J_{SC} values. The shunt resistance R_{shunt}, on the other hand accounts for the different charge recombination pathways (Karthick et al., 2020). The results seen in Fig. 8 were obtained with 0.7 μm absorber layer thickness, while the series resistance was varied from 10 to 100 Ω·cm^2, and the shunt resistance was varied from 500 to 5000 Ω·cm^2. The effect of the parasitic resistances was on the PCE, is shown in Fig. 8. Fig. 8 shows that the efficiency decreased from 14.5 % down to 2.12 % as the series resistance of the device increases from 10 to 100 Ω·cm^2 and the shunt resistance is increased from 1000 to 5000 Ω·cm^2.

Using a series resistances R_{series} of 10 Ω·cm^2 and the shunt resistance R_{shunt} of 5000 Ω·cm^2, the absorber thickness was again optimized against cell performance indicators: V_{OC}, FF, J_{SC} and η. The results are shown in Figs. 9-12.

Fig. 12 above shows that a maximum cell efficiency for the non-ideal device of 14.5 % is found in the absorber thickness range between 0.62 μm and 0.72 μm and a comparative table showing the difference in cell performance between the ideal and non-ideal device is given in Table 3. Table 3 shows that the efficiency drops from 21.0 % down to 14.5 % after parasitic resistances are introduced. Both the open-circuit voltage and the short-circuit current density decrease slightly compared to maximum value obtained in the ideal case. The largest decrease is seen in the fill factor, which dropped from 86.1 to 66.5 % when parasitic resistances were introduced. The absorber thickness associated with the maximum efficiency also decreased from 0.68 to 0.78 μm in the ideal device to 0.62–0.72 μm in the non-ideal device.

Several research works have reported on the influence of perovskite absorber thickness on cell efficiency (Du et al., 2016); (Rahman, et al., 2019); (De Los Santos, 2020). A comparison of PSC efficiency and the

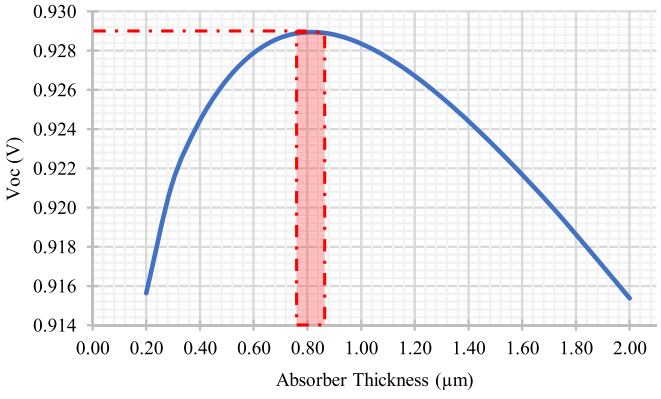

Fig. 4. Effect of absorber thickness on open-circuit voltage of an ideal device.

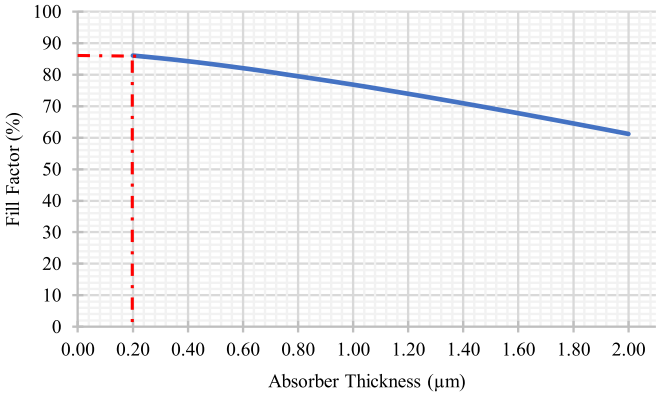

Fig. 5. Effect of absorber thickness on fill factor of an ideal device.

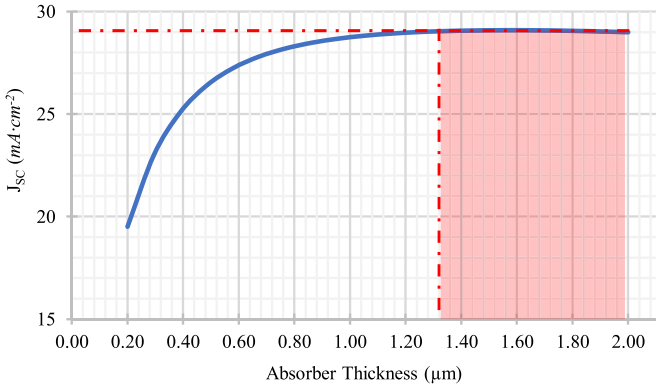

Fig. 6. Effect of absorber thickness on short- circuit current density of an ideal device.

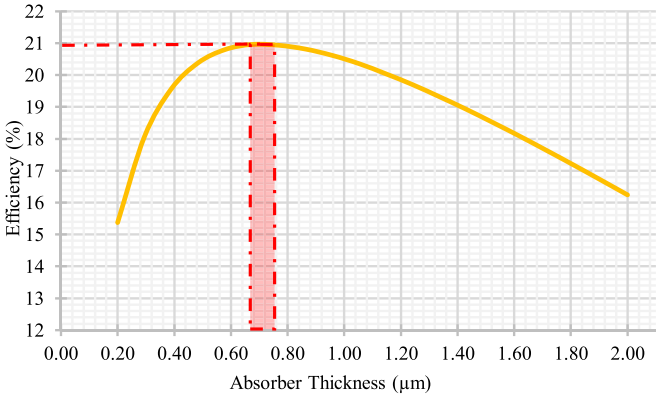

Fig. 7. Effect of absorber thickness on ideal cell efficiency of an ideal device.

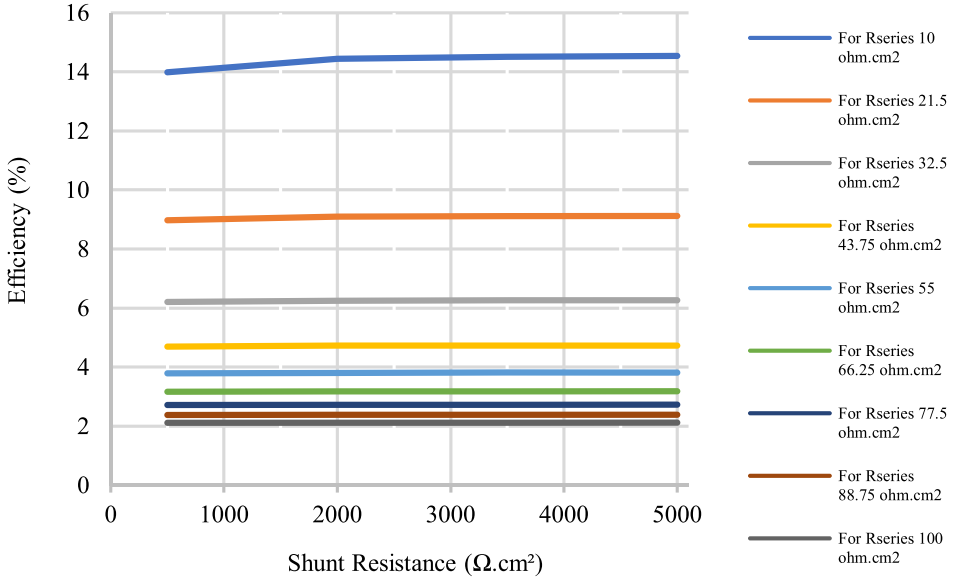

Fig. 8. Effect of shunt and series resistance on cell efficiency.

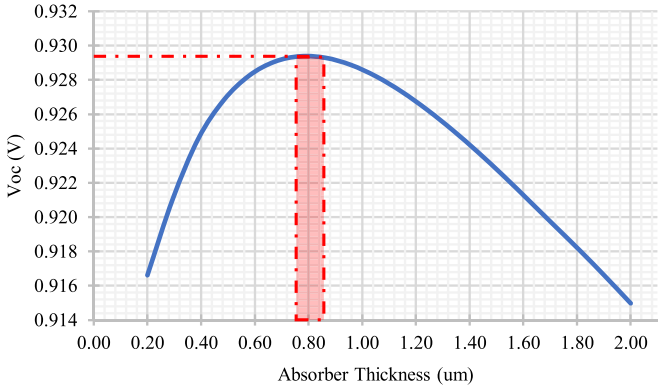

Fig. 9. Effect of absorber thickness on open- circuit voltage for non-ideal device.

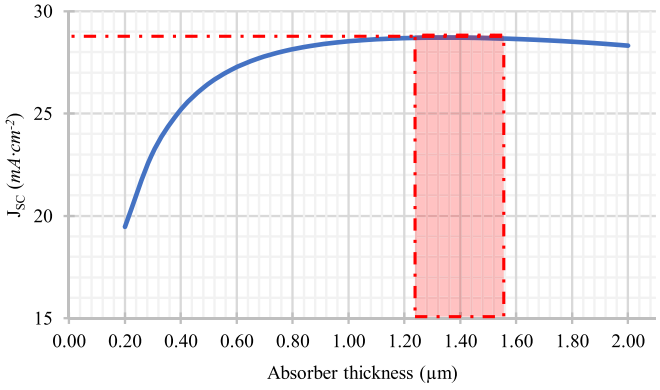

Fig. 11. Effect of absorber thickness on short- circuit current density for non-ideal device.

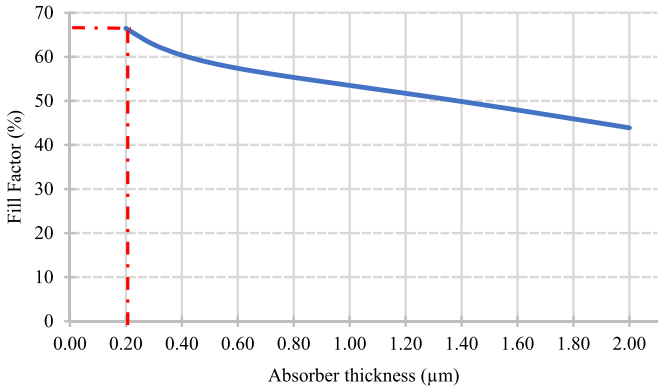

Fig. 10. Effect of absorber thickness on fill factor for non-ideal device.

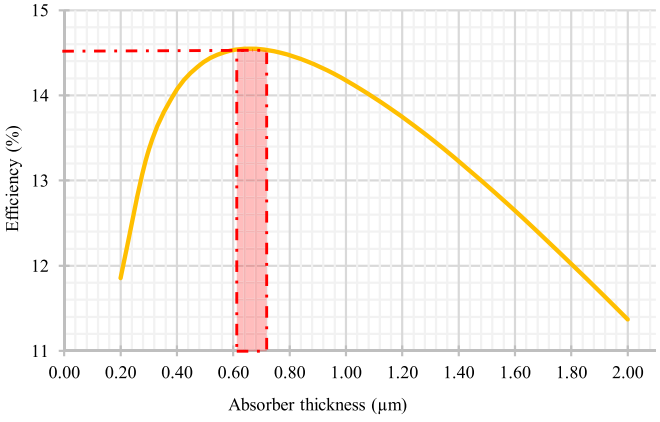

Fig. 12. Effect of absorber thickness on non-ideal cell efficiency.

thickness or defect density results for ideal and non-ideal device structures are shown in Table 4 and Table 5, respectively. The simulation-based studies by Karthick *et al.,* (Karthick et al., 2020) for the structure that is similar to the one presented in this paper except the LiTFSI-doped spiro-OMeTAD and the Ag metal contact resulted in 21.4 % PCE for the ideal device, achieved at a 0.35 µm active layer thickness. This PCE is comparable to the maximum efficiency 21.0 % in this study. The comparison in Table 5 shows that the 14.5 % PCE achieved in this paper agree with previous published results, with an efficiency ranging from 11.5 % to 16.5 %. The 100-fold increase in hole mobility in the HTL did not increase the PCE significantly. Table 5 also highlights the large

Table 3
Comparison between idea and non-ideal solar cell performance.

Performance Indicator	Optimal Value obtained	
	Ideal Device	Non-ideal Device (Expt*)
V_{oc}(V)	0.93	0.93 (0.6)
FF(%)	86.07	66.45 (40.6)
J_{sc}(mA·cm^{-2})	29.09	28.71 (16.6)
η (%)	20.95	14.45 (4.3)

*Experimental values taken from (Karthick et al., 2020).

Table 4
Comparison of results for ideal device between this work and previous publications.

Device Structure	Absorber Thickness (μm)	Efficiency (%)	Reference
SnO_2/$FAPbI_3$/Spiro-OMeTAD: LiTFSI	0.68–0.78	20.8*	This work
SnO_2/$MAPbI_3$/NiO_x	0.6–0.7	19.3*	(Rahman, et al., 2019)
TiO_2/$MAPbI_3$/NiO_x	0.6–0.7	18.4*	(Rahman, et al., 2019)
ZnO/$MAPbI_3$/NiO_x	0.6–0.7	19.7*	(Rahman, et al., 2019)
SnO_2/$FAPbI_3$/Spiro-OMeTAD	0.35	21.4*	(Karthick et al., 2020)
SnO_2/$FA_{0.85}$ $Cs_{0.15}$ PbI_3/ Spiro-OMeTAD	0.35	21.0*	(Karthick et al., 2020)
SnO_2/$FA_{0.85}$ $Cs_{0.15}$ $PbI_{0.85}Br_{0.15})_3$/Spiro-OMeTAD	0.35	18.7*	(Karthick et al., 2020)

*Indicates results are simulation based.

Table 5
Comparison of results for non-idea device between this work and previous publications.

Device Structure	Absorber Thickness (μm)	Efficiency (%)	Reference
SnO_2/$FAPbI_3$/Spiro-OMeTAD: LiTFSI	0.62–0.72	14.5*	This work
TiO_2/$CH_3NH_3SnI_3$/ Spiro-OMeTAD	0.6	16.5*	(Du et al., 2016)
TiO_2/$FASnI_3$/ Spiro-OMeTAD	0.35	14.03*	(Abdelaziz, 2020)
SnO_2/$FAPbI_3$/Spiro-OMeTAD	0.35	4.3**	(Karthick et al., 2020)
SnO_2/$FAPbI_3$/Spiro-OMeTAD	0.35	11.5*	(Karthick et al., 2020)
SnO_2/$FA_{0.85}$ $Cs_{0.15}$ PbI_3/ Spiro-OMeTAD	0.35	9.9**	(Karthick et al., 2020)
SnO_2/$FA_{0.85}$ $Cs_{0.15}$ PbI_3/ Spiro-OMeTAD	0.35	14.5*	(Karthick et al., 2020)
SnO_2/$FA_{0.85}$ $Cs_{0.15}$ $PbI_{0.85}Br_{0.15})_3$/Spiro-OMeTAD	0.35	15.1**	(Karthick et al., 2020)
SnO_2/$FA_{0.85}$ $Cs_{0.15}$ $PbI_{0.85}Br_{0.15})_3$/Spiro-OMeTAD	0.35	14.7**	(Karthick et al., 2020)

*Indicates results are simulation based.
**Indicates results are experimental based.

discrepancies between the 11.5 % simulated PCE and the 4.3 % experimental value for the same device (Karthick et al., 2020).

However, such a high PCE of the ideal device at a relatively smaller active layer thickness obtained by Karthick *et al* was achieved at a smaller active layer defect N_t of $4 \times 10^{13} cm^{-3}$ when compared to the $9 \times 10^{14} cm^{-3}$ used in this work. Table 6 shows a comparison of the defect level in the absorber layer and the corresponding efficiency attained for

Table 6
Comparison of absorber defects density with associated efficiency.

Device Structure	Absorber defect density, N_t (cm^{-3})	Efficiency (%)	Reference
SnO_2/$FAPbI_3$/Spiro-OMeTAD: LiTFSI	9.0 x 10^{14}	20.8*	This work
SnO_2/$MAPbI_3$/NiO_x	1.5 x 10^{16}	19.3*	(Rahman, et al., 2019)
SnO_2/$FAPbI_3$/Spiro-OMeTAD	4.0 x 10^{13}	21.4*	(Karthick et al., 2020)

*Indicates results are simulation based.

the device. Evidently, a high defect density in the absorber layer will lower the efficiency of PSC's with otherwise similar architectures.

This work shows that there is a narrow thickness range between 0.62 μm and 0.72 μm for the absorber material of the device to produce the maximum efficiency. In this section, we will explore the underlying theory supporting these results and the limitations of the simulation model. Firstly, an adequate active layer thickness is required to ensure satisfactory absorption of light. The absorption coefficient α(λ) is a function of wavelength in SCAPS 1-D (Burgelman, 2021), the optical absorption model is governed by the following equation:

$$\alpha(\lambda) = \left(A + \frac{B}{hf}\right)\sqrt{hf - E_g} \tag{1}$$

where, A and B are the model absorption parameters, usually set to 1×10^5 and$B = 0$, respectively, h is Planck's constant, f is frequency of the photons, and E_g is the energy gap of the material. Using the square root model means the absorption coefficient of the $FAPbI_3$ active layer in the visible spectrum range from $1 \times 10^5 cm^{-2}$ to $4.62 \times 10^4 cm^{-2}$. The absorption coefficient affects the charge carrier generation rate (G) (Bowden and Honsberg, 2019) in the device, given as as:

$$G = \alpha N_0 e^{-\alpha x} \tag{2}$$

where N_0 is the number of incident photons, x is distance into the material. The short-circuit current density which is approximated (Bowden and Honsberg, 2019) as:

$$J_{SC} = qG(L_n + L_p) \tag{3}$$

here, q is the electronic charge, L_n (L_p) is the electron (hole) diffusion length given in as

$$L_{n,p} = \sqrt{\frac{kT\mu_{n,p}\tau}{q}} \tag{4}$$

where,$k$is Boltzmann's constant, μ_n $\left(\mu_p\right)$ is electron (hole) mobility, and τ is the carrier lifetime (s), which is defined by

$$\tau = \frac{1}{\sigma \times N_t \times v_{th}} \tag{5}$$

where,σ is carrier capture cross section $\left(m^2\right)$, N_t is the defect density $\left(m^{-3}\right)$, v_{th} is the carrier thermal velocity.

Eqs. (1)-(3) describe how the short-circuit current is proportional to both the rate of pair generation, including α dependence and the charge carrier diffusion lengths. Both Figs. 6 and 11 clearly show that the short-circuit current density needs to reach a certain thickness of absorber in order to be optimal. Without sufficient active layer thickness, the absorber material is not able to absorb enough photons and there is low photogeneration of charge carriers and J_{SC}. Fig. 7 and Fig. 12 show that above thicknesses of 0.78 μm and 0.72 μm the efficiency will start to decline for the ideal and non-ideal device, respectively. When the thickness is greater than the diffusion length, then the electrons and holes recombine before leaving the absorber material. Charge carriers

cannot travel the entire width of the material before slipping back into a lower energy state as a recombined pair. The diffusion length of the charge carriers determines the upper limit to the optimized thickness. The calculated L_p for $FAPbI_3$ active layer is 0.72 μm, which lies in the optimized thickness range found in both the ideal and non-ideal device simulations.

The influence of parasitic losses on the device can be understood using Eq. (6) (Karthick et al., 2020; Li, 2017):

$$I = I_L - I_0\left[e^{\frac{q(M)}{nkT}} - 1\right] - \left(\frac{M}{R_{shunt}}\right) \quad (6)$$

where, I_L is the light-induced current, $M = V + (I \times R_{series})$, I_0 is the reverse saturation current of the diode, and n is ideality factor. According to Eq. (6), a small R_{series} and large R_{shunt} are required for high PCE. Karthick *et al* used experimentalR_{series} = 88.3 Ω·cm^2 andR_{shunt} = 710.0 Ω·cm^2 based on 0.2 cm^2 solar cell area and the PCE dropped from 21.4 % to 11.5 % compared to the 14.5 % in this work. This indicates that improvements in charge carrier transport and collection at the electrodes, coupled with optimized active layer thickness can increase the PCE of the device by 26 %. These results underscore the importance of optimization in solar cell design.

4. Conclusions

We have optimized the active layer of an n-i-p PSC with the structure FTO/SnO_2/$FAPbI_3$/Spiro-MeTAD:LiTFSI/(Ag) using SCAPS-1D simulation software. An efficiency of 20.95 % was achieved in the ideal device for the optimized $FAPbI_3$ thickness from 0.67 μm to 0.77 μm. In the non-ideal device, an efficiency of 14.45 % was achieved when the absorber layer thickness was between 0.62 μm and 0.72 μm. The design was based on an experiment PSC with a PCE of 4.3 %. The present study shows that the performance of the original non-ideal design can be improved by optimization of layer thickness and carrier transport to achieve 28.71 mA·cm^{-2} short-circuit current density, 66.45 % fill factor reached, 0.93 V open-circuit voltage, and 14.45 % PCE, which is a 26 % increase from the 11.5 % of the non-ideal design.

5. Role of the funding source

This research did not receive any specific grant from funding agencies in the public, commercial, or not-for-profit sectors.

CRediT authorship contribution statement

David Ompong: Conceptualization, Methodology, Formal analysis, Validation, Supervision, Writing – review & editing. **Michelle Clements:** Conceptualization, Data curation, Writing – review & editing, Formal analysis, Validation, Visualization.

Declaration of competing interest

The authors declare that they have no known competing financial interests or personal relationships that could have appeared to influence the work reported in this paper.

Data availability

Data will be made available on request.

Acknowledgments

The authors will like to thank Dr. Marc Burgelman of the University of Gent in Belgium for providing the SCAPS simulation program.

References

Abdelaziz, S., et al., 2020. Investigating the performance of formamidinium tin-based perovskite solar cell by SCAPS device simulation. Opt. Mater. 101 (109738).
Bowden, S.G. and C.B. Honsberg, Photovoltaics Education Website. 2019.
Burgelman, M., et al., 2021. SCAPS Manual. University of Gent, Belgium.
Burgelman, M., Nollet, P., Degrave, S., 2000. Modelling polycrystalline semiconductor solar cells. Thin Solid Films 361–362, 527–532.
Chen, L.-C., Tseng, Z.-L., Huang, J.-K., 2016. A study of inverted-type perovkite solar cells with various composition ratios of (FAPbI3)1–x(MAPbBr 3)x. Nanomaterials 6 (183).
Chouhan, A.S., Jasti, N.P., Avasthi, S., 2018. Effect of interface defect density of performance of perovskite solar cell: correlation of simulation and experiment. Mater. Lett. 221, 150–153.
De Los Santos, I.M., et al., 2020. Optimization of CH3NH3PbI3 perovskite solar cells: a theoretical and experimental study. Sol. Energy 199, 198–205.
Ding, Y., et al., 2022. Single-crystalline TiO2 nanoparticles for stable and efficient perovskite modules. Nat. Nanotechnol.
Djurisic, A.B., et al., 2017. Perovskite solar cells - an overview of critical issues. Prog. Quantum Electron. 53, 1–37.
Du, H.J., Wang, W.C., Zhu, J.Z., 2016. Device simulation of lead-free CH3NH3SnI3 perovskite solar cells with high efficiency. Chin. Phys. B 25 (10).
Gelvez-Rueda, M., Renaud, N., Grozema, F.C., 2017. Temperature depenedent charge carrier dynamics in formamidiniyum lead iodide perovskite. The Journal Physical Chemistry 121, 23392–23397.
Głowienka, D., et al., 2020. Role of surface recombination in perovskite solar cells at the interface of HTL/CH3NH3PbI3. Nano Energy 67, 104186.
Hao, F., et al., 2014. Lead-free solid-state organic-inorganic halide perovskite solar cells. Nat. Photonics 8, 489–494.
Hima, A., et al., 2019. An optimized perovskite solar cell designs for high conversion efficiency. Superlattice. Microst. 129, 240–246.
Karthick, S., Velumani, S., Boucle, J., 2020. Experimental and SCAPS simulated formadinium perovskite solar cells: a comparison of device performance. Sol. Energy 205, 349–357.
Karthick, S., Bouclé, J., Velumani, S., 2021. Effect of bismuth iodide (BiI3) interfacial layer with different HTL's in FAPI based perovskite solar cell – SCAPS – 1D study. Sol. Energy 218, 157–168.
Li, Y., et al., 2017. Ultra-high open-circuit voltage of perovskite solar cells induced by nucleation thermodynamics on rough substrates. Sci. Rep. 7 (1), 46141.
Li, B., et al., 2020. Insights into the hole transport properties of LiTFSI-doped spiro-OmeTAD films through impedance spectroscopy. J. Appl. Phys. 128 (085501).
Ma, F., et al., 2017. Stable a/d phase junction of formamidinium lead iodide perovskites for enhanced near-infrared emission. Chem. Sci. 8, 800–805.
Manser, J.S., Christians, J.A., Kamat, P.V., 2016. Intriguing optoelectronic properties of metal halide perovskites. Chem. Rev. 116 (21), 12956–13008.
Mercaldo, L.V., et al., 2022. Procedure Based on external quantum efficiency for reliable characterization of perovskite solar cells. Energ. Technol. 10 (10), 2200748.
Ompong, D., Singh, J., 2018. High open-circuit voltage in perovskite solar cells: the role of hole transport layer. Org. Electron. 63, 104–108.
Ono, L.K., et al., 2017. Perovskite solar cells—towards commercialization. ACS Energy Lett. 2 (8), 1749–1751.
Rahman, S., et al. Simulation based Investigation of Inverted Planar Perovskite Solar Cell with All Metal Oxide Inorganic Transport Layers. 7-9 February, 2019.
Shao, S., Loi, M.A., 2020. The role of the interfaces in perovskite solar cells. Adv. Mater. Interf. 7 (1), pp.
Song, Z., et al., 2016. Pathways toward high-performance perovskite solar cells: review of recent advances in organo-metal halide perovskites for photovoltaic applications. SPIE.
Tockhorn, P., et al., 2020. Improved quantum efficiency by advanced light management in nanotextured solution-processed perovskite solar cells. ACS Photonics 7 (9), 2589–2600.
Whalley, L.D., et al., 2017. Perspective: theory and simulation of hybrid halide perovskites. J. Chem. Phys. 146 (22), 220901.